

Lattice thermal conductivity and elastic modulus of XN_4 ($\text{X}=\text{Be}$, Mg and Pt)

2D materials using machine learning interatomic potentials

K. Ghorbani¹, P. Mirchi^{1,2}, S. Arabha^{1,3}, and Ali Rajabpour^{1,4*}, Sebastian Volz^{5,6*}

¹ Advanced Simulation and Computing Laboratory (ASCL), Imam Khomeini International University, Qazvin, Iran.

² Department of Mechanical Engineering, K. N. Toosi University of Technology, Tehran, Iran.

³ Department of Mechanical Engineering, Lassonde School of Engineering, York University, Toronto M3J 1P3, Canada.

⁴ School of Nano Science, Institute for Research in Fundamental Sciences (IPM), Tehran, Iran.

⁵ Institute of Industrial Science, The University of Tokyo, Tokyo 153-8505, Japan.

⁶LIMMS, CNRS-IIS IRL 2820, The University of Tokyo, Tokyo 153-8505, Japan.

Abstract

The newly synthesized BeN_4 monolayer has introduced a novel group of 2D materials called nitrogen-rich 2D materials. In the present study, the anisotropic mechanical and thermal properties of three members of this group, BeN_4 , MgN_4 , and PtN_4 , are investigated. To this end, a machine learning-based interatomic potential (MLIP) is developed on the basis of the moment tensor potential (MTP) method and utilized in classical molecular dynamics (MD) simulation. Mechanical properties are calculated by extracting the stress-strain curve and thermal properties by non-equilibrium molecular dynamics (NEMD) method. Acquired results show the anisotropic elastic modulus and lattice thermal conductivity of these materials. Generally, elastic modulus and thermal conductivity in the armchair direction are higher than in the zigzag direction. Also, the elastic anisotropy is almost constant at every temperature for BeN_4 and MgN_4 , while for PtN_4 , this parameter is decreased by increasing the temperature. The findings of this research are not only evidence of the application of machine learning in MD simulations, but also provide information on the basic anisotropic mechanical and thermal properties of these newly discovered 2D nanomaterials.

* Corresponding authors: A. Rajabpour, Email: rajabpour@eng.ikiu.ac.ir S. Volz, Email: volz@iis.u-tokyo.ac.jp

1- Introduction

By the fabrication of graphene as the first two-dimensional (2D) material in 2004 [1], developing novel materials of this kind and investigating their properties and behavior have attracted considerable attention from researchers in various fields of science, ranging from chemistry and physics to engineering. Today, a wide range of 2D materials (e.g. phosphorene [2], borophene [3] h-BN [4]–[7], black phosphorene [8], [9], and MoS₂ [10], [11]) with distinguished mechanical, thermal, electrical and optical properties has been introduced. In addition to the properties of these materials, their geometry also makes them as promising structures with potential application in nanoelectronics and optoelectronics.

Generally, experimental study is the main approach in investigating the behavior and properties of materials and structures, but when it comes to micro/nanoscales', due to their submicron dimensions, using this approach encounters remarkable restrictions. So, theoretical and computer simulation-based methods in this regard have been remarked rapidly, particularly, after recent notable advances in computational tools. Molecular Dynamics (MD) simulation and density functional theory (DFT) are of the methods in this regard that have been successfully implemented in modeling of various systems including vibration behavior [12]–[17], mechanical and thermal properties [18]–[27], and electronic properties [28]–[31]. DFT is a time-consuming method providing the highest accurate results, while MD simulation is less time-consuming but its results firmly rely on the interatomic potential functions. Machine-learning methods provide an opportunity to develop specific potential functions for each desired simulation leading to highly accurate results in the range of DFT results with less computational cost. Mortazavi et al. [32]–

[36] conducted various research on investigating the mechanical and thermal properties of micro/nano-scale materials through developing machine-learning interatomic potentials (MLIPs). Recently, Arabha et al. [37] published a comprehensive review paper on the application of MLIPs in the calculation of lattice thermal conductivity. In this study, thermal conductivity of different 2D and 3D materials obtained from various approaches including experiment, DFT, MD, and MLIP has been compared and the significance of developing MLIP was indicated. Also, different machine-learning techniques in creating interatomic potentials and their characteristics were presented in this paper. Zuo et al. [38] in a comprehensive comparison study analyzed the efficiency and the computational costs of different MLIPs including MTP, SNAP, qSNAP, NNP, and GAP for Cu and Ni fcc metals, Li and Mo bcc metals, and Si and Ge semiconductors which are the representative of various material/structural properties. Accordingly, it can be said that all MLIPs in comparison to classical interatomic potentials provide the highest accuracy in estimating the energies/forces and properties. Botu et al. [39] presented a workflow and five main steps in generating MLIPs.

The interfacial thermal conductance across C_3N , C_3B , C_2N , C_3N_4 , and C_3N_4 carbon-based 2D structures was also investigated [40]. Mortazavi et al. [41] proposed a new computational approach to compute a phonon dispersion relation and analyze the dynamical stability of nanomaterials. This approach is based on a machine-learning interatomic potentials and provides faster and more efficient results than the DFT simulations. The usefulness of this approach has been presented for a wide range of low-symmetry and porous 2D nanomaterials.

Arabha and Rajabpour [42] investigated the thermal conductivity and Young's modulus of nitrogenated holey graphene (C_2N) using MLIPs. The significant dependency of thermal conductivity on length was reported in their work. They have also evaluated the development of

MLIPs for the point-defected C_2N structures. They have shown, while there is uncertainty in the stability of point-defected C_2N structures using Tersoff classical interatomic potential, that the MLIP is able to well calculate the properties of these structures.

Recently, the synthesis of BeN_4 [43] introduced a new group of 2D materials called nitrogen-rich 2D materials with XN_4 chemical formulation in which X is the representative of metallic elements [28]. Thereafter, Mortazavi et al. [28] analyzed the stability and the mechanical, thermal, electronic, and phononic properties of a wide range of these 2D materials including BeN_4 , MgN_4 , IrN_4 , RhN_4 , NiN_4 , CuN_4 , AuN_4 , PdN_4 , and PtN_4 by conducting the DFT calculations. They have reported that among the observed materials only BeN_4 , MgN_4 , IrN_4 , PtN_4 and RhN_4 have the required dynamical and thermal stability. Also, it has been shown that the mechanical properties of BeN_4 , MgN_4 , PtN_4 and RhN_4 are sensitive to the armchair and zigzag directions so that the armchair ones have a higher elastic modulus and tensile strength than those in zigzag structures. Berdiyrov et al. [44] investigated the anisotropic electronic properties of BeN_4 and MgN_4 using the DFT and non-equilibrium Green's functional methods. They have indicated that in comparison to zigzag direction, the armchair direction provides remarkably larger electronic charge transport capability. Tong et al. [45], [46] determined the anisotropic phonon and electron thermal conductivity of BeN_4 at room temperature and at high and ambient pressures utilizing the combination of Boltzmann transport equation and first-principle calculations. Cheng et al. investigated the lattice thermal conductivity of layered Dirac semimetal BeN_4 using the Boltzmann transport equation and first-principles three-phonon calculations [47]. Wang et al. [48] used first-principles simulations to investigate the thermal properties of BeN_4 and MgN_4 .

In the present study, a machine learning-based interatomic potential is developed and employed in MD simulations for investigating the mechanical properties and thermal conductivity of BeN_4 ,

MgN₄, and PtN₄ 2D monolayers shown in Figure 1. The main steps in this regard are as follows. Firstly, the ab-initio molecular dynamic trajectories are obtained as the subsample set, and then, the interatomic potential is trained over this subsample using the momentum tensor potential (MTP) machine learning method. Finally, utilizing the trained interatomic potential in the MD simulation, the desired mechanical and thermal properties are calculated.

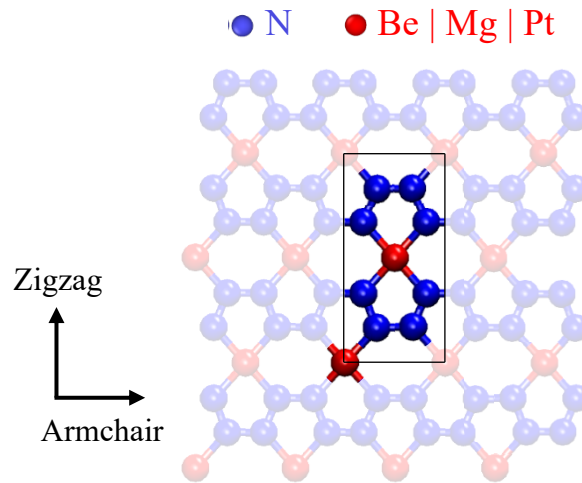


Figure 1. Atomic structure of BeN₄, MgN₄, and PtN₄ 2D monolayers and their corresponding armchair and zigzag directions.

2- Methodology

In this section, the process of extracting the machine learning-based interatomic potentials using the ab- initio molecular dynamic (AIMD) results and MTP method proposed by Shapeev [49], and utilizing them in classical MD simulations to calculate the mechanical properties and thermal conductivity of BeN₄, MgN₄, and PtN₄ will be discussed.

2.1 Ab-initio simulation

The aim of implementing ab-initio simulations is to produce the necessary dataset sources for training the MLIPs. To this end, structures are firstly optimized for seven different strains between 0-14% and nine various temperatures between 100-1000 K. It should be noted, all simulation was performed 1000 times steps of 1 fs, in every strain and temperature.

2.2 Interatomic potential training

Here, the MLIPs are developed using the MTP [49]. According to this method, the interatomic potentials can be defined as a multiplication of inertia tensors of radial polynomial functions. In order to train the parameters of MTP, the difference between the obtained results from the first principle calculations (i.e. energy, forces, and stresses) and the predicted results is minimized [49], [50]:

$$\sum_{m=1}^M \left[w_e (E_m^{AIMD} - E_m^{MTP})^2 + w_f \sum_i^N |f_{m,i}^{AIMD} - f_{m,i}^{MTP}|^2 + w_s \sum_{i,j}^N |\sigma_{m,ij}^{AIMD} - \sigma_{m,ij}^{MTP}|^2 \right] \quad (1)$$

$\rightarrow min$

In this equation, m is the number of training set configurations and N is the total number of atoms. E_m , $f_{m,i}$, and $\sigma_{m,i}$ are respectively energy, force, and stress terms, and AIMD and MTP superscripts indicate the corresponding values obtained from AIMD modeling and MTP calculations. Also, w_e , w_f , and w_s are the positive weighted coefficients showing the significance of energy, force, and stress expressions, and are considered to be 1, 0.1, and 0.001, respectively. For the initial training subsample sets, 10% of the AIMD calculated trajectories at first are considered in this regard. That is due to the fact that the correlation of the calculated trajectories are done in a short-range time. Then, MTP is trained over these initial subsample sets. By assessing the accuracy of the trained MTP over all of the AIMD trajectories, the subsample sets are updated

by the high degree of extrapolation trajectories [51], and again MTP is trained over these new subsample sets. The algorithm of training the MLIPs is indicated in Figure 2. The ultimate trained MTP is considered as the MLIP and used in MD simulations.

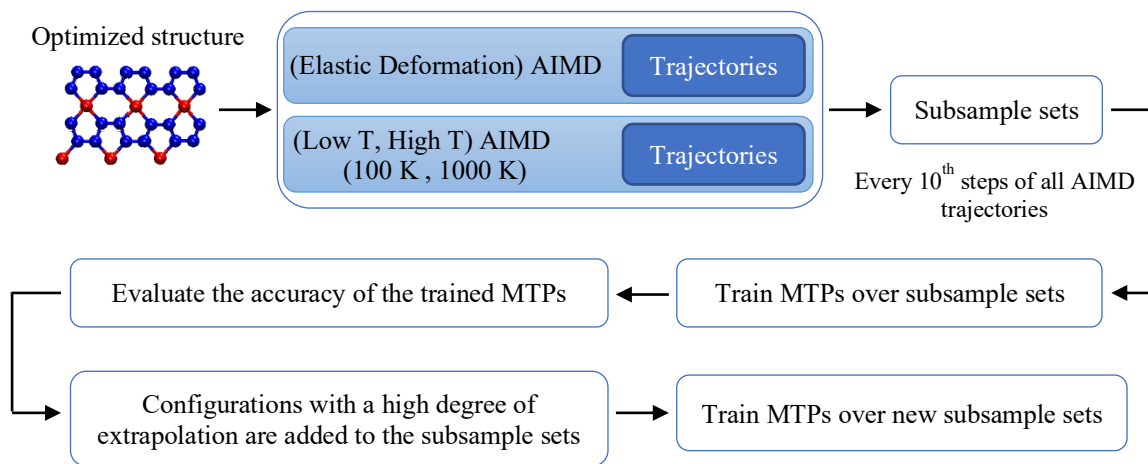


Figure 2. Machine-learning interatomic potentials (MLIPs) training algorithm. [42]

2.3 Molecular dynamic simulations

In this paper, MD simulations are performed using a Large-scale Atomic/Molecular Massively Parallel Simulator (LAMMPS) package [52], and the MTP trained potential as the interatomic potential, with 0.5 fs time-step and 300K average temperature. Also, the boundary conditions are periodic which remove the surface effects at boundaries and minimize the influence of finite-length.

The lattice thermal conductivity of desired materials is calculated based on the non-equilibrium molecular dynamics (NEMD) [53][54][55][56] method. To this end, at first by the use of Nose-Hoover barostat and thermostat (NPT) at room temperature, the nanostructures are relaxed for 2.5 ps. Then, the heat flux is imposed in the equilibrated structures by creating a temperature gradient between the defined hot and cold regions at the end sides of the structures, as shown in Figure 3.

The added and subtracted average energy from the two baths are calculated in the microcanonical ensemble (NVE) for 3ns. At the end, the thermal conductivity is calculated using Fourier's law of heat conduction as follows:

$$\kappa = -q'' / \frac{dT}{dx} \quad (2)$$

In which q'' is the heat flux through the structure and $\frac{dT}{dx}$ is the temperature gradient within it.

In order to compute the mechanical properties, the simulation box at first is stretched in the direction of loading at a specific engineering strain rate of $1 \times 10^9 \text{ S}^{-1}$, and then by plotting the stress-strain curve, the slop in the linear region is reported as the Young's modulus of the structure.

Based on the virial theorem, the stress values are obtained as follows [57]:

$$S = \frac{1}{V} \sum_{a \in V} \left[-m \vec{v}_a \otimes \vec{v}_a + \frac{1}{2} \sum_{a \neq b} (\vec{r}_{ab} \otimes \vec{F}_{ab}) \right] \quad (3)$$

in which, S represents the stress tensor and V is the volume of structure. m and \vec{v}_a are the mass and velocity vector, respectively. Also, \vec{r}_{ab} and \vec{F}_{ab} indicate the position and force vectors between atoms a and b , and \otimes denotes the outer product.

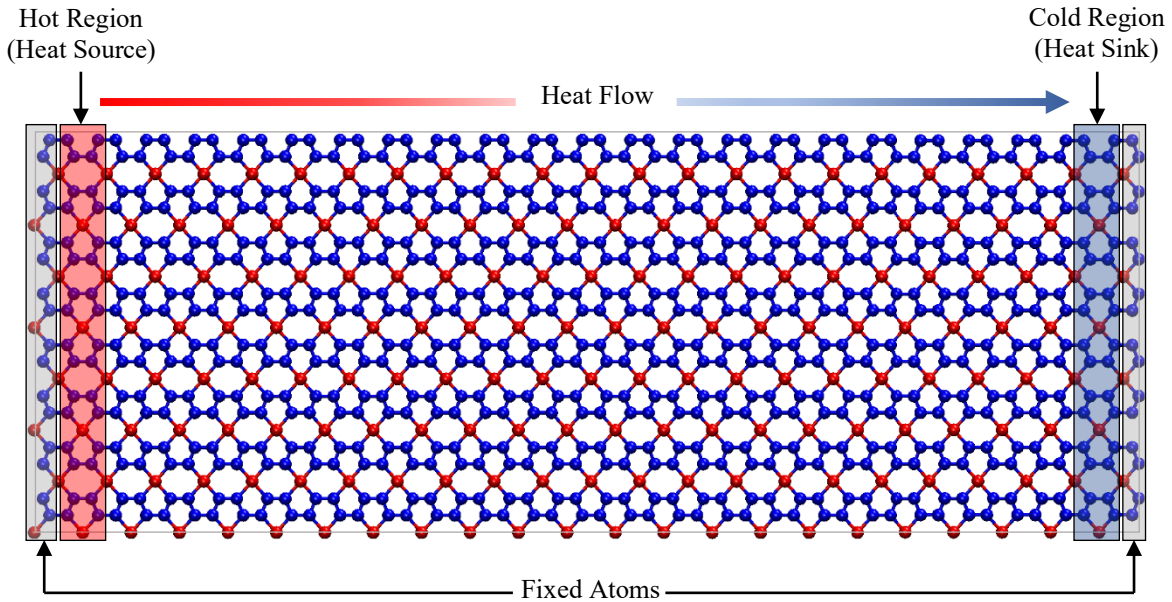


Figure 3. Schematic illustration of the NEMD setup for the calculation of thermal conductivity

3- Results and discussion

The main focus of the present research is the calculation of thermal and mechanical properties of BeN_4 , MgN_4 , and PtN_4 monolayers using the MD simulation and MLIP. The acceptable data set for training the MLIP must consist in all the possible trajectories that a system may experience in MD simulation. So, to generate training data sets, a wide range of temperature, from 100 K to 1000 K, is considered for the AIMD simulations. This range of temperature provides trajectories with both long-wavelength phonons, related to low-temperature conditions, and high-frequency optical modes, related to high-temperature conditions. Also, the high-temperature AIMD trajectories are needed for the consideration of large local deformations that probably happen in NEMD simulations of long-length structures.

Before presenting the thermal and mechanical properties, the dynamical stability of the considered structures is examined through the phonon dispersion relations (PDR) obtained from MLIP-based

MD simulations using mlip_phonopy scripts [41]. As illustrated in Figure 4, no imaginary frequencies appear in the PDR, which confirms the dynamical stability of BeN₄, MgN₄, and PtN₄ 2D monolayers. Moreover, PDR predicted by DFT is shown in Figure S1 (Supplementary data).

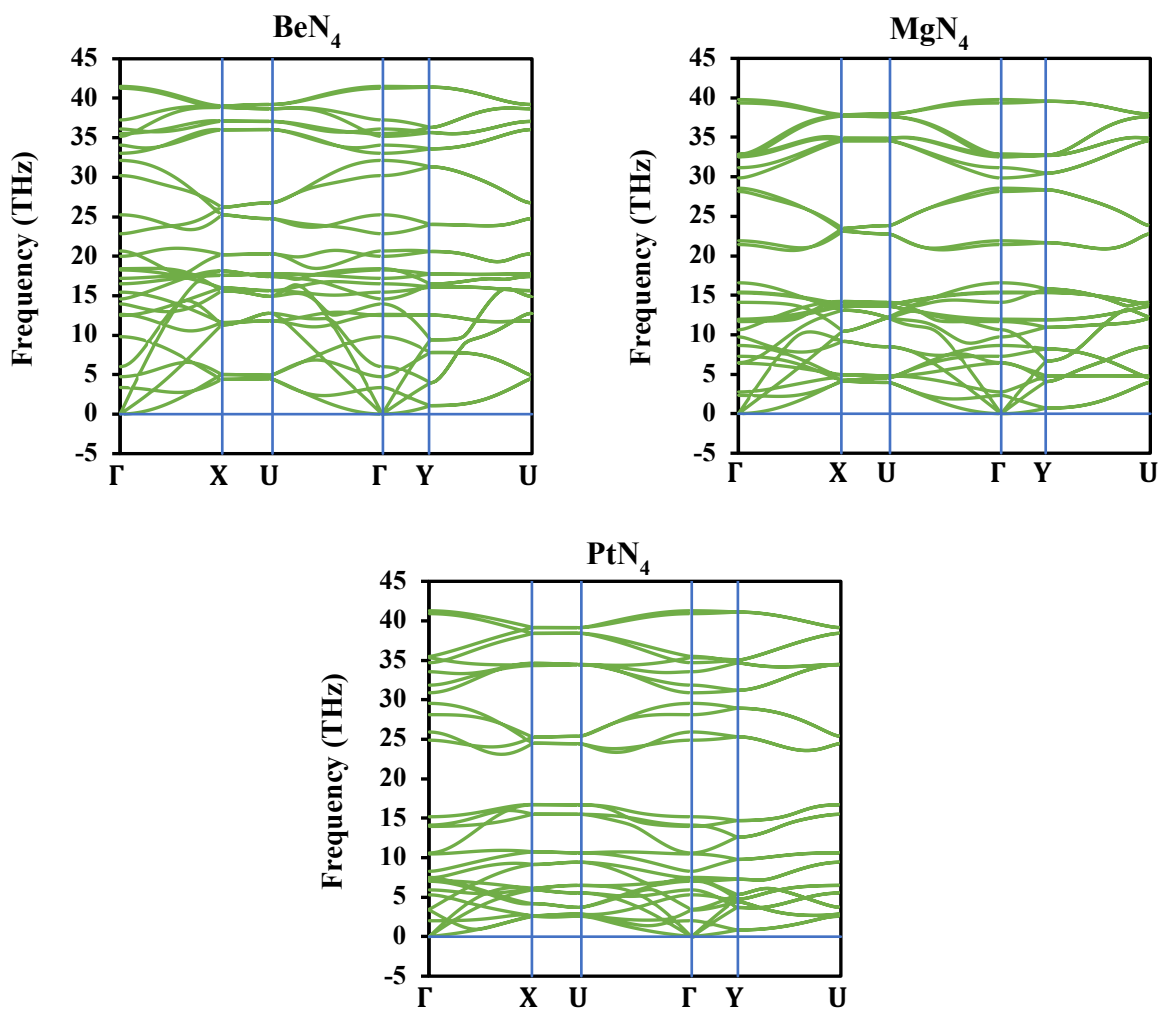


Figure 4. Phonon dispersion relations of BeN₄, MgN₄, and PtN₄ 2D monolayers.

3.1 Thermal properties

By implementing the trained MLIP in NEMD simulations, the lattice thermal conductivity of BeN₄, MgN₄, and PtN₄ 2D nano sheets in the armchair and zigzag directions has been investigated.

In Figure 5 the variation of thermal conductivity versus length in both armchair and zigzag directions is shown. As can be seen in this figure, for all these three materials and in both directions, the thermal conductivity at short lengths is length-dependent so that by increasing the length, the thermal conductivity increases. But, as the length increases, this dependency decreases and thermal conductivity converges to a specific value at longer lengths. The values of thermal conductivity in both directions are presented in the same figure.

From a comparative point of view, it can be seen that the BeN₄ monolayer has the highest thermal conductivity in both directions with ~140 and ~ 107 W/m-K in armchair and zigzag directions respectively, while the lowest values of this property in armchair and zigzag directions belong to the PtN₄ monolayers with ~ 115 and ~ 41 W/m-K respectively. Also, the change rate of thermal conductivity relative to length is different in armchair and zigzag directions and there is a significant difference in the values of thermal conductivity between these two directions. In other words, it can be stated that in thermal applications, the orientation of these 2D materials is of great importance. It should be noted that the thermal conductivity at infinite length, k_{∞} , is approximated through fitting of the well-known equation $1/k_L = (1 + \Lambda/L)/k_{\infty}$ [58] on the calculated thermal conductivity at finite lengths, k_L . In this equation Λ is the effective phonon mean free path.

The observed thermal behavior is justifiable by analyzing the phonon group velocity as the main criteria of lattice thermal conductivity variation. To this end, the phonon group velocity of BeN₄, MgN₄, and PtN₄ are plotted in Figure 6. Also, in this figure the phonon group velocity of graphene as a benchmark is presented. The phonon group velocities at low-frequency modes are generally considered as the main heat carrier. As it is obvious in this figure, at low-frequency modes, BeN₄ and PtN₄ respectively have the highest and lowest phonon group velocities that is the indicative of

their thermal conductivity. This result is completely aligned with the obtained lattice thermal conductivity.

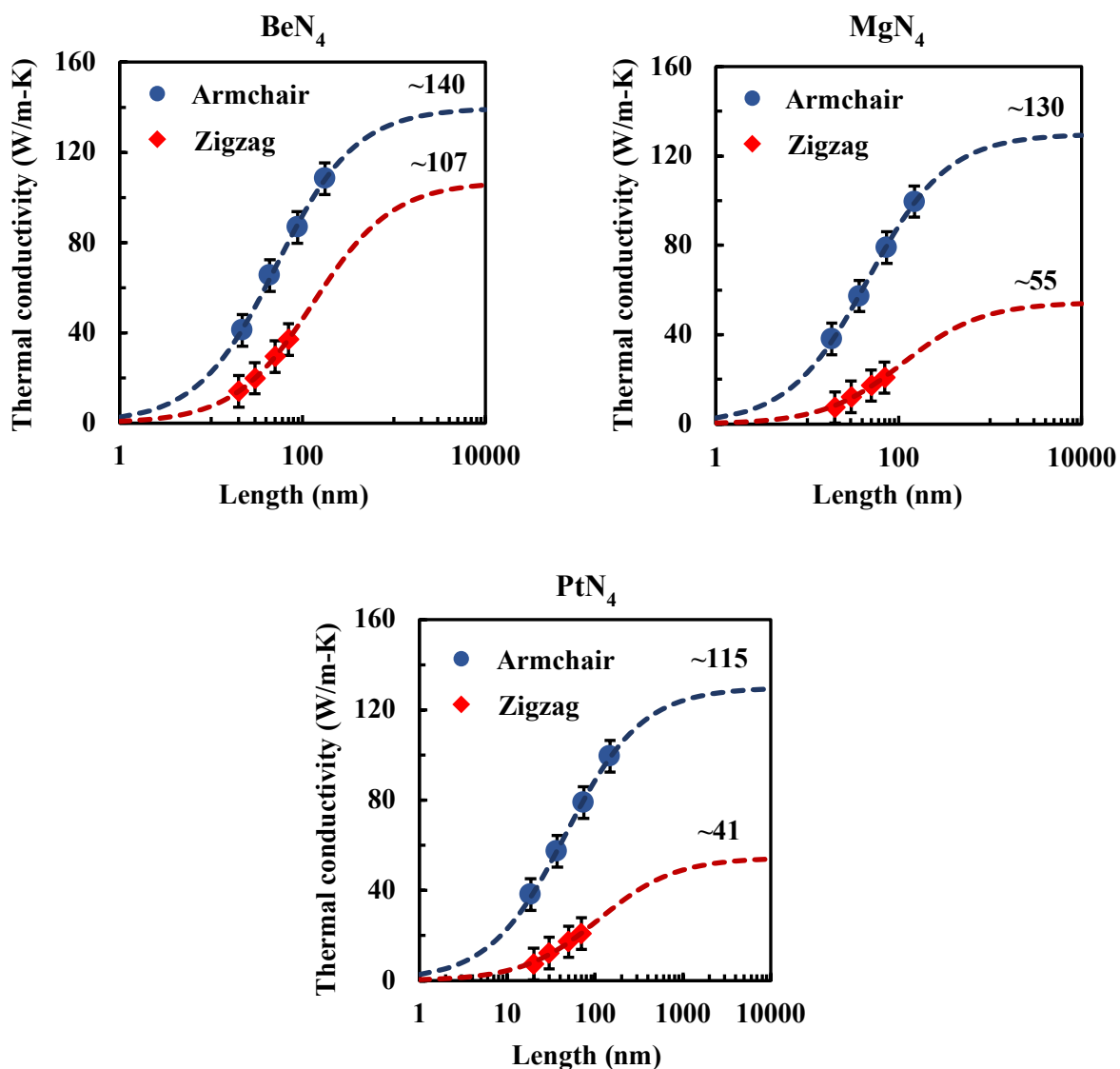


Figure 5. The variation of lattice thermal conductivity as a function of length at 300K.

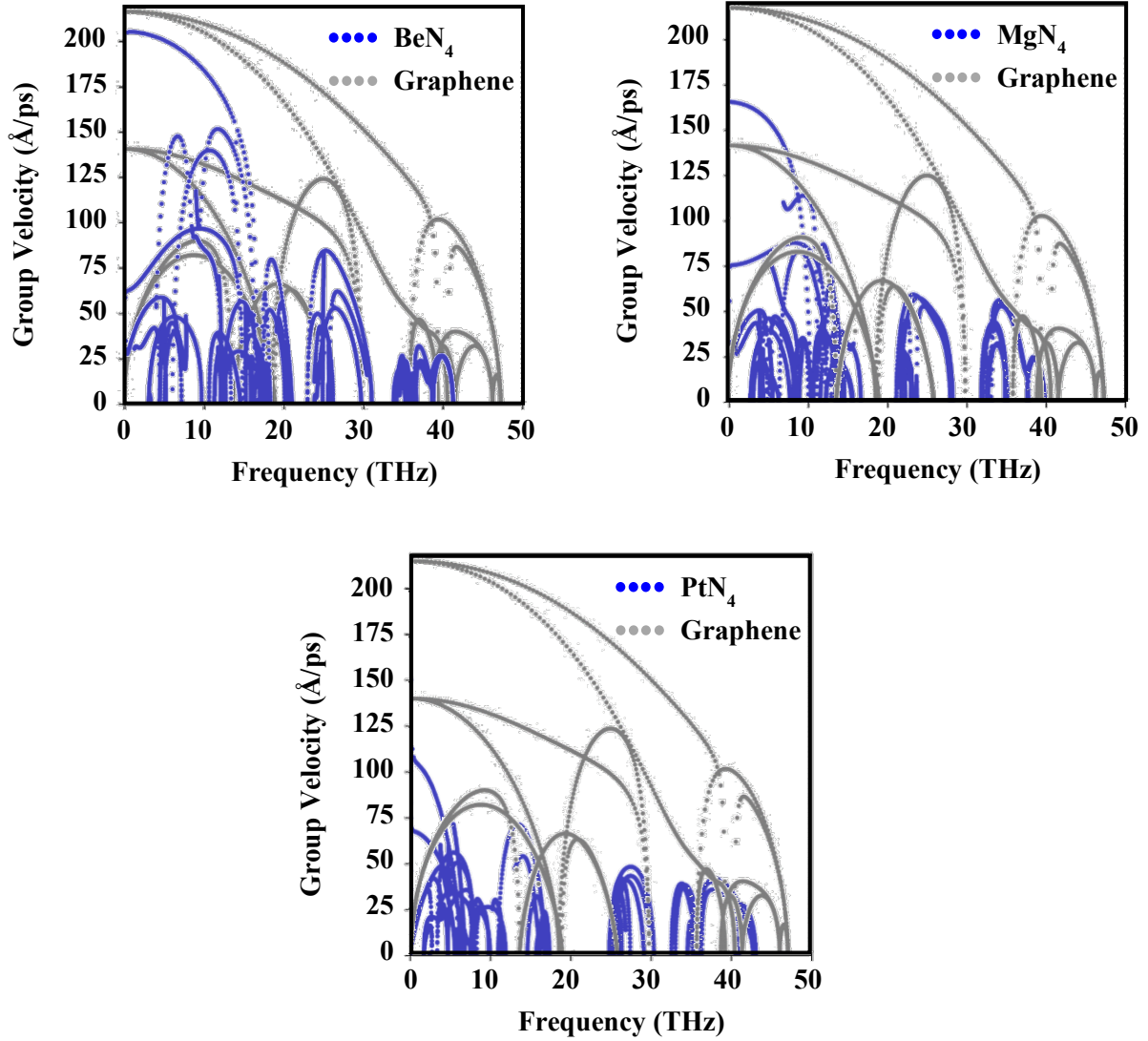


Figure 6. Phonon group velocity. Comparison of BeN₄, MgN₄, and PtN₄ with graphene.

3.2 Mechanical properties

In this subsection, temperature and chirality-dependent mechanical properties of BeN₄, MgN₄, and PtN₄ 2D materials obtained from classical MD simulations with the trained interatomic potential will be discussed. To this end, the uniaxial stress-strain relation in armchair and zigzag directions of these materials (see Figure 1) at room temperature is evaluated and shown in Figure 7. It should be noted that the thickness of structures is assumed to be 3.06 Å. According to this figure, it can

be said that for these 2D materials, the ultimate strength in the zigzag direction is generally lower than those of armchair ones. Also, as can be concluded from this figure, the ultimate strength of BeN₄, MgN₄, and PtN₄ in the armchair direction are approximately close together (with about 70, 76, and 76 GPa respectively). The same conclusion is not valid in the zigzag direction so that just the ultimate strength of BeN₄ and MgN₄ (\approx 40 GPa) are similar in this direction while for PtN₄ the value of this property is about 70 GPa. The reason for such a behavior and generally for the anisotropic mechanical behavior of these structures is rooted in the dominant bonds that have to be broken during the uniaxial loading. As it is clear in Figure 1, the N-N bond is perfectly aligned in the armchair direction so in the case of uniaxial loading along this direction, it can be said that initiation of the bond failure as the criterion in calculating the ultimate strength depends mostly on N-N bonds regardless of the type of metallic atoms (Be, Mg, and Pt) in the structure. On the other hand, in the zigzag direction, the Be-N, Mg-N, and Pt-N bonds play a dominant role so that the type of metallic atoms has an influence on the ultimate strength.

In contrast to MgN₄, the fracture strain in the zigzag direction is higher than their armchair counterparts. Also, it can be deduced from this figure that MgN₄ and BeN₄ have the highest and lowest values of fracture strain respectively.

In Figure 8, the variation of elastic modulus versus temperature has been presented. The dependency of elastic modulus on chirality and temperature is obvious in this figure. As illustrated in this figure, armchair structures have higher values of elastic modulus than the ones of the zigzag structures, and by increasing the temperature, the elastic modulus decreases in both armchair and zigzag directions. Moreover, it can be noticed that both armchair and zigzag structures of MgN₄ have the lowest values of elastic modulus, while interestingly, the highest values of this property are associated with the BeN₄ in armchair direction and PtN₄ in the zigzag direction. The elastic

modulus of BeN₄, MgN₄, and PtN₄ along the armchair (zigzag) directions presented in Figure 9 corresponds to a 13% (23%), 11% (17%), and 13% (10%) difference from those reported in Ref [28], respectively. The different input data sizes and strain ranges employed in AIMD may be the cause of these discrepancies.

In order to examine the dependency of anisotropic behavior on temperature, the variation of anisotropy relative to temperature is plotted in Figure 10. Here, anisotropy is defined as $\frac{E_a - E_z}{E_a}$ where E_a and E_z are the elastic modulus along the armchair and zigzag directions respectively. As can be seen in this figure, for BeN₄ and MgN₄, the anisotropy is about 0.4 and almost constant at any temperature, while for PtN₄, the anisotropy is less than 0.2 and decreases by increasing the temperature. This behavior is also obvious in Figure 8 more specifically for PtN₄. So, it can be stated that BeN₄ and MgN₄ display an anisotropic mechanical behavior at each temperature but PtN₄ shows an isotropic mechanical behavior at high temperatures.

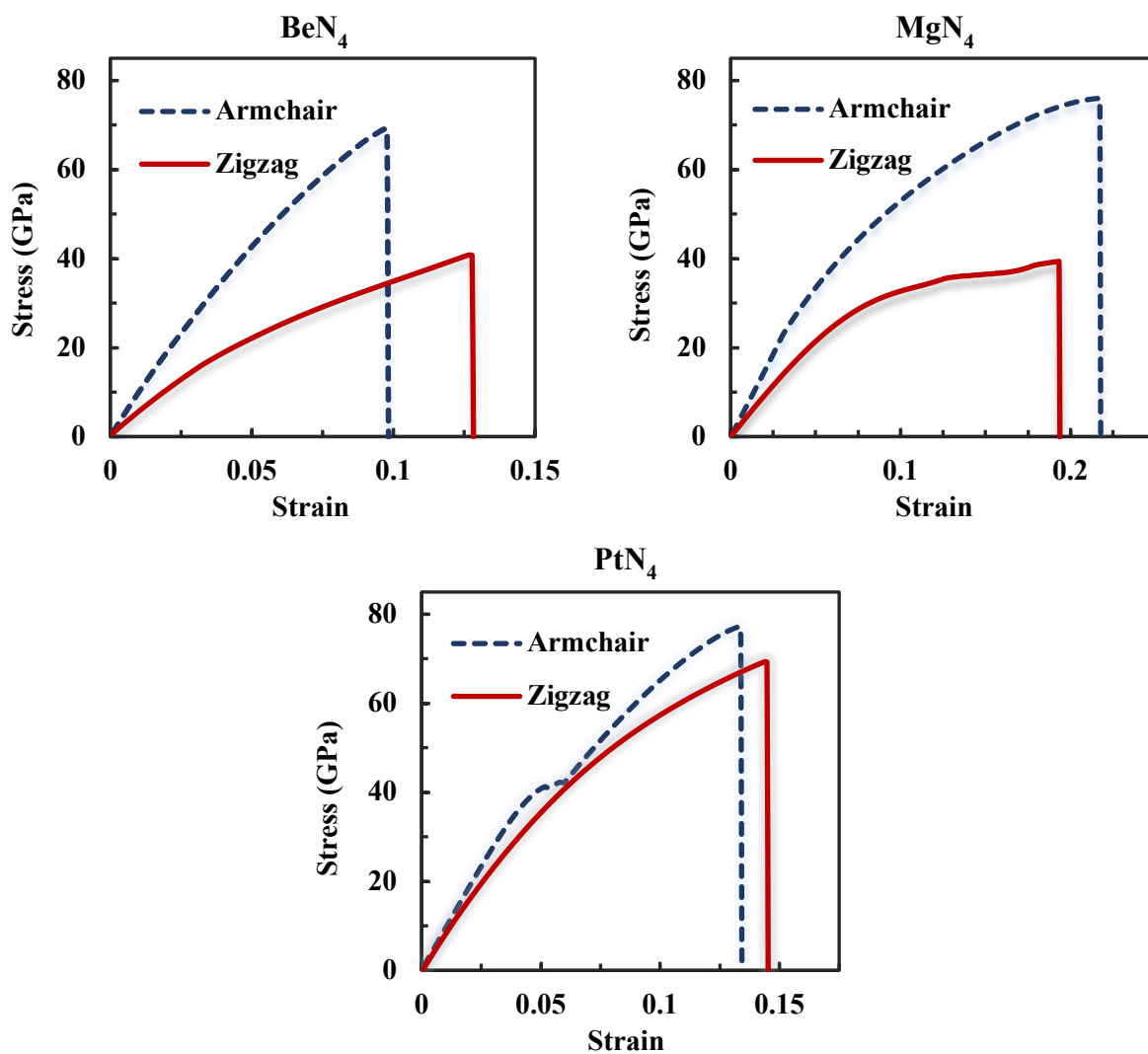


Figure 7. Stress-strain diagram under uniaxial tensile load at 300K.

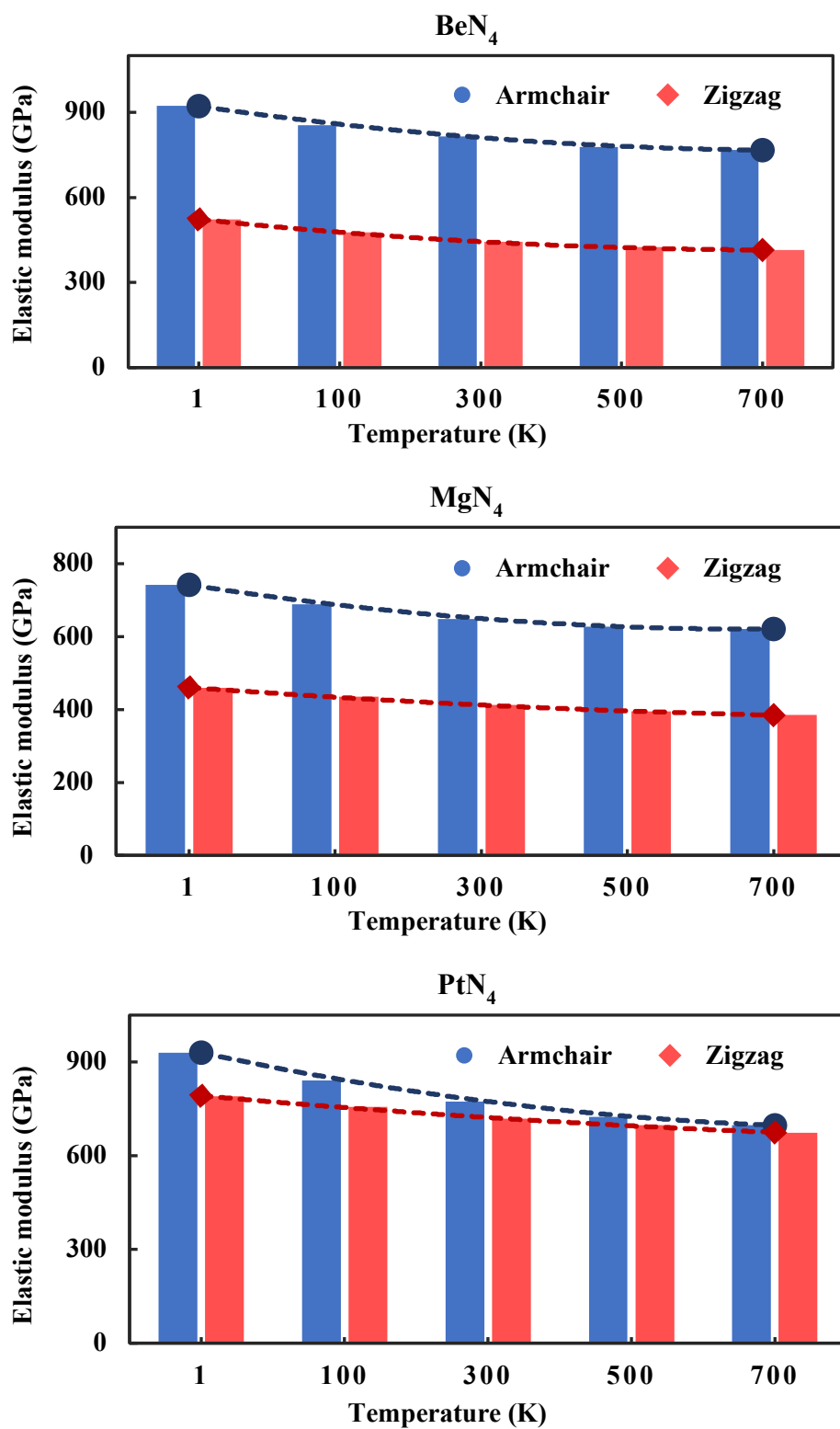


Figure 8. The variation of elastic modulus as a function of temperature.

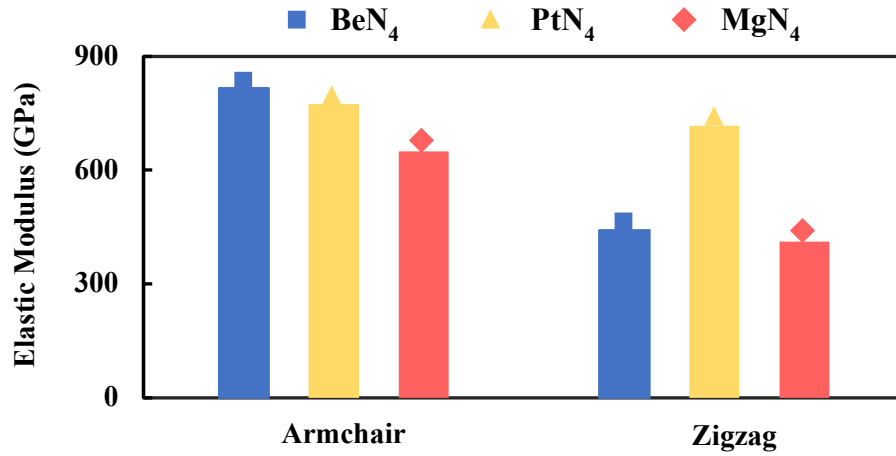


Figure 9. Comparison of elastic moduli of BeN₄, MgN₄, and PtN₄ in armchair and zigzag directions at 300K

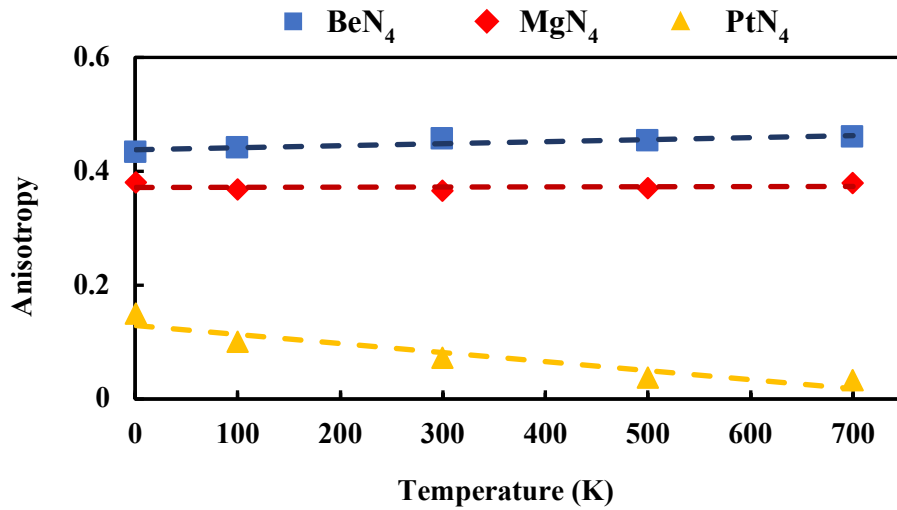


Figure 10. Dependency of elastic modulus anisotropy on temperature.

4- Conclusion

In summary, the present study provided details on the anisotropic mechanical and thermal properties of BeN₄, MgN₄, and PtN₄ monolayers, a new group of 2D materials. This aim was achieved by developing a MLIP using MTP method, and MD simulation. The anisotropic elastic

modulus and lattice thermal conductivity are concluded from the results in such a way that armchair orientation leads to higher elastic modulus and thermal conductivity than the ones in the zigzag orientation. Also, the anisotropy ($\frac{E_a - E_z}{E_a}$) in BeN₄ and MgN₄ is independent of temperature and is approximately constant. However, increasing the temperature reduces anisotropy in PtN₄. Moreover, thermal conductivity increases by increasing the length and at long lengths, it reaches a constant value so that BeN₄ present the highest thermal conductivity in armchair and zigzag directions, and PtN₄ exhibits the lowest values in both directions. On the other hand, the order from highest to lowest values of elastic moduli follows BeN₄, PtN₄, and MgN₄, in the armchair direction and PtN₄, BeN₄, and MgN₄ in the zigzag direction, while this trend for thermal conductivity is BeN₄, MgN₄, and PtN₄ in both directions.

Furthermore, the present study is an evidence of the application of machine learning approach in developing interatomic potential functions and use them in classical MD simulations yielding the highest accuracy with less computational costs.

Acknowledgment

This work is based upon research funded by Iran National Science Foundation (INSF) under project No. 4002089.

References

- [1] K. S. Novoselov *et al.*, “Electric Field Effect in Atomically Thin Carbon Films,” *Science* (1979), vol. 306, no. 5696, pp. 666–669, 2004, doi: 10.1126/science.1102896.
- [2] L. Z. Li, S. Han, W. M. Wang, H. Tan, and Q. Zhou, “A New Approach for Gray Image Segmentation Using Level Set Method,” in *Advances in Measurements and Information Technologies*, 2014, vol. 530, pp. 372–376. doi: 10.4028/www.scientific.net/AMM.530-531.372.

- [3] A. J. Mannix *et al.*, “Synthesis of borophenes: Anisotropic, two-dimensional boron polymorphs,” *Science (1979)*, vol. 350, no. 6267, pp. 1513–1516, 2015, doi: 10.1126/science.aad1080.
- [4] K. Watanabe, T. Taniguchi, and H. Kanda, “Direct-bandgap properties and evidence for ultraviolet lasing of hexagonal boron nitride single crystal,” *Nat Mater*, vol. 3, no. 6, pp. 404–409, 2004.
- [5] Y. Kubota, K. Watanabe, O. Tsuda, and T. Taniguchi, “Deep Ultraviolet Light-Emitting Hexagonal Boron Nitride Synthesized at Atmospheric Pressure,” *Science (1979)*, vol. 317, no. 5840, pp. 932–934, 2007, doi: 10.1126/science.1144216.
- [6] J.-H. Park *et al.*, “Large-Area Monolayer Hexagonal Boron Nitride on Pt Foil,” *ACS Nano*, vol. 8, no. 8, pp. 8520–8528, 2014, doi: 10.1021/nn503140y.
- [7] K. Zhang, Y. Feng, F. Wang, Z. Yang, and J. Wang, “Two dimensional hexagonal boron nitride (2D-hBN): synthesis, properties and applications,” *J Mater Chem C Mater*, vol. 5, no. 46, pp. 11992–12022, 2017, doi: 10.1039/C7TC04300G.
- [8] L. Li *et al.*, “Black phosphorus field-effect transistors,” *Nat Nanotechnol*, vol. 9, no. 5, pp. 372–377, 2014, doi: 10.1038/nnano.2014.35.
- [9] K. Cai, J. Wan, N. Wei, H. Cai, and Q.-H. Qin, “Thermal stability of a free nanotube from single-layer black phosphorus,” *Nanotechnology*, vol. 27, no. 23, p. 235703, Apr. 2016, doi: 10.1088/0957-4484/27/23/235703.
- [10] C. Donnet, J. M. Martin, Th. Le Mogne, and M. Belin, “Super-low friction of MoS₂ coatings in various environments,” *Tribol Int*, vol. 29, no. 2, pp. 123–128, 1996, doi: [https://doi.org/10.1016/0301-679X\(95\)00094-K](https://doi.org/10.1016/0301-679X(95)00094-K).
- [11] J. P. Oviedo *et al.*, “In Situ TEM Characterization of Shear-Stress-Induced Interlayer Sliding in the Cross Section View of Molybdenum Disulfide,” *ACS Nano*, vol. 9, no. 2, pp. 1543–1551, Feb. 2015, doi: 10.1021/nn506052d.
- [12] K. Ghorbani, A. Rajabpour, and M. Ghadiri, “Determination of carbon nanotubes size-dependent parameters: molecular dynamics simulation and nonlocal strain gradient continuum shell model,” *Mechanics Based Design of Structures and Machines*, vol. 49, no. 1, pp. 103–120, 2021, doi: 10.1080/15397734.2019.1671863.
- [13] K. Mohammadi, A. Rajabpour, and M. Ghadiri, “Calibration of nonlocal strain gradient shell model for vibration analysis of a CNT conveying viscous fluid using molecular dynamics simulation,” *Comput Mater Sci*, vol. 148, pp. 104–115, 2018, doi: <https://doi.org/10.1016/j.commatsci.2018.02.036>.
- [14] A. Akbarshahi, A. Rajabpour, M. Ghadiri, and M. M. Barooti, “Influence of various setting angles on vibration behavior of rotating graphene sheet: continuum modeling and molecular dynamics simulation,” *J Mol Model*, vol. 25, no. 5, p. 141, 2019, doi: 10.1007/s00894-019-3996-5.

- [15] M. Ghadiri, A. Rajabpour, and A. Akbarshahi, “Non-linear vibration and resonance analysis of graphene sheet subjected to moving load on a visco-Pasternak foundation under thermo-magnetic-mechanical loads: An analytical and simulation study,” *Measurement*, vol. 124, pp. 103–119, 2018, doi: <https://doi.org/10.1016/j.measurement.2018.04.007>.
- [16] S. Ajori, S. Haghghi, H. Parsapour, and R. Ansari, “Fundamental frequency analysis of endohedrally functionalized carbon nanotubes with metallic nanowires: a molecular dynamics study,” *J Mol Model*, vol. 27, no. 11, p. 313, 2021, doi: 10.1007/s00894-021-04933-8.
- [17] S. Ajori, F. Sadeghi, and R. Ansari, “Dynamic behavior of chloride ion-electrically charged open carbon nanocone oscillators: A molecular dynamics study,” *Proc Inst Mech Eng C J Mech Eng Sci*, vol. 235, no. 21, pp. 5709–5717, 2021, doi: 10.1177/0954406220984504.
- [18] M. Mirnezhad, R. Ansari, and S. R. Falahatgar, “Quantum effects on the mechanical properties of fine-scale CNTs: an approach based on DFT and molecular mechanics model,” *The European Physical Journal Plus*, vol. 135, no. 11, p. 908, 2020, doi: 10.1140/epjp/s13360-020-00878-8.
- [19] M. Mirnezhad, R. Ansari, S. R. Falahatgar, and P. Aghdasi, “Torsional buckling analysis of MWCNTs considering quantum effects of fine scaling based on DFT and molecular mechanics method,” *J Mol Graph Model*, vol. 104, p. 107843, 2021, doi: <https://doi.org/10.1016/j.jmngm.2021.107843>.
- [20] S. M. Hatam-Lee, H. Peer-Mohammadi, and A. Rajabpour, “Tuning shear mechanical properties and tensile strength anisotropy of monolayer black phosphorene: A molecular dynamics study,” *Mater Today Commun*, vol. 26, p. 101796, 2021, doi: <https://doi.org/10.1016/j.mtcomm.2020.101796>.
- [21] M. Roodbari, M. Abbasi, S. Arabha, A. Gharedaghi, and A. Rajabpour, “Interfacial thermal conductance between TiO₂ nanoparticle and water: A molecular dynamics study,” *J Mol Liq*, p. 118053, 2021, doi: <https://doi.org/10.1016/j.molliq.2021.118053>.
- [22] F. Hasheminia, Y. Bahari, A. Rajabpour, and S. Arabha, “Elucidation of thermo-mechanical properties of silicon nanowires from a molecular dynamics perspective,” *Comput Mater Sci*, vol. 200, p. 110821, 2021, doi: <https://doi.org/10.1016/j.commatsci.2021.110821>.
- [23] A. Rajabpour, R. Seif, S. Arabha, M. M. Heyhat, S. Merabia, and A. Hassanali, “Thermal transport at a nanoparticle-water interface: A molecular dynamics and continuum modeling study,” *J Chem Phys*, vol. 150, no. 11, p. 114701, 2019, doi: 10.1063/1.5084234.
- [24] M. M. Heyhat, A. Rajabpour, M. Abbasi, and S. Arabha, “Importance of nanolayer formation in nanofluid properties: Equilibrium molecular dynamic simulations for Ag-

- water nanofluid,” *J Mol Liq*, vol. 264, pp. 699–705, 2018, doi: <https://doi.org/10.1016/j.molliq.2018.05.122>.
- [25] Q. Bao, Z. Yang, Z. Lu, and X. He, “Effects of graphene thickness and length distribution on the mechanical properties of graphene networks: A coarse-grained molecular dynamics simulation,” *Appl Surf Sci*, vol. 570, p. 151023, 2021, doi: <https://doi.org/10.1016/j.apsusc.2021.151023>.
- [26] T. Zhou *et al.*, “Thermal transport in amorphous small organic materials: a mechanistic study,” *Phys. Chem. Chem. Phys.*, vol. 22, no. 5, pp. 3058–3065, 2020, doi: 10.1039/C9CP05938E.
- [27] Y. He, I. Savić, D. Donadio, and G. Galli, “Lattice thermal conductivity of semiconducting bulk materials: atomistic simulations,” *Phys. Chem. Chem. Phys.*, vol. 14, no. 47, pp. 16209–16222, 2012, doi: 10.1039/C2CP42394D.
- [28] B. Mortazavi, F. Shojaei, and X. Zhuang, “Ultrahigh stiffness and anisotropic Dirac cones in BeN₄ and MgN₄ monolayers: a first-principles study,” *Mater Today Nano*, vol. 15, p. 100125, 2021, doi: <https://doi.org/10.1016/j.mtnano.2021.100125>.
- [29] B. Mortazavi, M. Shahrokhi, X. Zhuang, T. Rabczuk, and A. V Shapeev, “Mechanical, thermal transport, electronic and photocatalytic properties of penta-PdPS, -PdPSe and -PdPTe monolayers explored by first-principles calculations,” *J Mater Chem C Mater*, vol. 10, no. 1, pp. 329–336, 2022, doi: 10.1039/D1TC05297G.
- [30] R. M. Tromer, L. C. Felix, C. F. Woellner, and D. S. Galvao, “A DFT investigation of the electronic, optical, and thermoelectric properties of pentadiamond,” *Chem Phys Lett*, vol. 763, p. 138210, 2021, doi: <https://doi.org/10.1016/j.cplett.2020.138210>.
- [31] O.-K. Park *et al.*, “Hexagonal boron nitride-carbon nanotube hybrid network structure for enhanced thermal, mechanical and electrical properties of polyimide nanocomposites,” *Compos Sci Technol*, vol. 188, p. 107977, 2020, doi: <https://doi.org/10.1016/j.compscitech.2019.107977>.
- [32] B. Mortazavi, A. Rajabpour, X. Zhuang, T. Rabczuk, and A. V Shapeev, “Exploring thermal expansion of carbon-based nanosheets by machine-learning interatomic potentials,” *Carbon N Y*, 2022, doi: <https://doi.org/10.1016/j.carbon.2021.10.059>.
- [33] B. Mortazavi, E. V Podryabinkin, I. S. Novikov, T. Rabczuk, X. Zhuang, and A. V Shapeev, “Accelerating first-principles estimation of thermal conductivity by machine-learning interatomic potentials: A MTP/ShengBTE solution,” *Comput Phys Commun*, vol. 258, p. 107583, 2021.
- [34] B. Mortazavi, E. V Podryabinkin, S. Roche, T. Rabczuk, X. Zhuang, and A. V Shapeev, “Machine-learning interatomic potentials enable first-principles multiscale modeling of lattice thermal conductivity in graphene/borophene heterostructures,” *Mater Horiz*, vol. 7, no. 9, pp. 2359–2367, 2020, doi: 10.1039/d0mh00787k.

- [35] B. Mortazavi, M. Silani, E. V Podryabinkin, T. Rabczuk, X. Zhuang, and A. V Shapeev, “First-Principles Multiscale Modeling of Mechanical Properties in Graphene/Borophene Heterostructures Empowered by Machine-Learning Interatomic Potentials,” *Advanced Materials*, vol. 33, no. 35, p. 2102807, 2021, doi: 10.1002/adma.202102807.
- [36] B. Mortazavi, I. S. Novikov, and A. V Shapeev, “A machine-learning-based investigation on the mechanical/failure response and thermal conductivity of semiconducting BC₂N monolayers,” *Carbon N Y*, vol. 188, pp. 431–441, 2022, doi: <https://doi.org/10.1016/j.carbon.2021.12.039>.
- [37] S. Arabha, Z. S. Aghbolagh, K. Ghorbani, S. M. Hatam-Lee, and A. Rajabpour, “Recent advances in lattice thermal conductivity calculation using machine-learning interatomic potentials,” *J Appl Phys*, vol. 130, no. 21, p. 210903, 2021, doi: 10.1063/5.0069443.
- [38] Y. Zuo *et al.*, “Performance and Cost Assessment of Machine Learning Interatomic Potentials,” *Journal of Physical Chemistry A*, vol. 124, no. 4, pp. 731–745, 2020, doi: 10.1021/acs.jpca.9b08723.
- [39] V. Botu, R. Batra, J. Chapman, and R. Ramprasad, “Machine Learning Force Fields: Construction, Validation, and Outlook,” *The Journal of Physical Chemistry C*, vol. 121, no. 1, pp. 511–522, Jan. 2017, doi: 10.1021/acs.jpcc.6b10908.
- [40] S. M. Hatam-Lee, K. Gordiz, and A. Rajabpour, “Lattice-dynamics-based descriptors for interfacial heat transfer across two-dimensional carbon-based nanostructures,” *J Appl Phys*, vol. 130, no. 13, p. 135106, 2021, doi: 10.1063/5.0055708.
- [41] B. Mortazavi *et al.*, “Exploring phononic properties of two-dimensional materials using machine learning interatomic potentials,” *Appl Mater Today*, vol. 20, p. 100685, 2020, doi: 10.1016/j.apmt.2020.100685.
- [42] S. Arabha and A. Rajabpour, “Thermo-mechanical properties of nitrogenated holey graphene (C₂N): A comparison of machine-learning-based and classical interatomic potentials,” *Int J Heat Mass Transf*, vol. 178, 2021, doi: 10.1016/j.ijheatmasstransfer.2021.121589.
- [43] M. Bykov *et al.*, “High-Pressure Synthesis of Dirac Materials: Layered van der Waals Bonded $\{\mathrm{BeN}\}_4$ Polymorph,” *Phys. Rev. Lett.*, vol. 126, no. 17, p. 175501, Apr. 2021, doi: 10.1103/PhysRevLett.126.175501.
- [44] G. R. Berdiyrov, B. Mortazavi, and H. Hamoudi, “Anisotropic charge transport in 1D and 2D BeN₄ and MgN₄ nanomaterials: A first-principles study,” *FlatChem*, vol. 31, p. 100327, 2022, doi: <https://doi.org/10.1016/j.flatc.2021.100327>.
- [45] Z. Tong, A. Pecchia, C. Yam, H. Bao, T. Dumitrică, and T. Frauenheim, “Significant Increase of Electron Thermal Conductivity in Dirac Semimetal Beryllonitrene by Doping Beyond Van Hove Singularity,” *Adv Funct Mater*, vol. n/a, no. n/a, p. 2111556, doi: <https://doi.org/10.1002/adfm.202111556>.

- [46] Z. Tong, A. Pecchia, C. Yam, L. Zhou, T. Dumitrică, and T. Frauenheim, “Anisotropic Phononic and Electronic Thermal Transport in BeN₄,” *J Phys Chem Lett*, vol. 13, no. 20, pp. 4501–4505, May 2022, doi: 10.1021/acs.jpcllett.2c01104.
- [47] Y.-B. Cheng, Q. Li, and J. Zhou, “First-principles study on the lattice thermal conductivity of layered Dirac semimetal BeN₄,” *Physica E Low Dimens Syst Nanostruct*, vol. 147, p. 115571, Mar. 2023, doi: 10.1016/J.PHYSE.2022.115571.
- [48] M. Wang and D. Han, “Thermal Properties of 2D Dirac Materials MN₄(M = Be and Mg): A First-Principles Study,” *ACS Omega*, vol. 7, no. 12, pp. 10812–10819, Mar. 2022, doi: 10.1021/ACSOMEGA.2C00785/ASSET/IMAGES/LARGE/AO2C00785_0011.JPEG.
- [49] A. V Shapeev, “Moment tensor potentials: A class of systematically improvable interatomic potentials,” *Multiscale Modeling & Simulation*, vol. 14, no. 3, pp. 1153–1173, 2016.
- [50] I. S. Novikov, K. Gubaev, E. V Podryabinkin, and A. V Shapeev, “The MLIP package: moment tensor potentials with MPI and active learning,” *Mach Learn Sci Technol*, vol. 2, no. 2, p. 025002, 2021, doi: 10.1088/2632-2153/abc9fe.
- [51] E. V Podryabinkin and A. V Shapeev, “Active learning of linearly parametrized interatomic potentials,” *Comput Mater Sci*, vol. 140, pp. 171–180, 2017, doi: 10.1016/j.commatsci.2017.08.031.
- [52] S. Plimpton, “Fast parallel algorithms for short-range molecular dynamics,” *J Comput Phys*, vol. 117, no. 1, pp. 1–19, 1995, doi: 10.1006/jcph.1995.1039.
- [53] Y. Hu *et al.*, “Unification of nonequilibrium molecular dynamics and the mode-resolved phonon Boltzmann equation for thermal transport simulations,” *Phys. Rev. B*, vol. 101, no. 15, p. 155308, Apr. 2020, doi: 10.1103/PhysRevB.101.155308.
- [54] F. Müller-Plathe, “A simple nonequilibrium molecular dynamics method for calculating the thermal conductivity,” *Journal of Chemical Physics*, vol. 106, no. 14, pp. 6082–6085, 1997, doi: 10.1063/1.473271.
- [55] A. Rajabpour, S. M. Vaez Allaei, and F. Kowsary, “Interface thermal resistance and thermal rectification in hybrid graphene-graphane nanoribbons: A nonequilibrium molecular dynamics study,” *Appl Phys Lett*, vol. 99, no. 5, p. 51917, 2011, doi: 10.1063/1.3622480.
- [56] B. Mortazavi and S. Ahzi, “Thermal conductivity and tensile response of defective graphene: A molecular dynamics study,” *Carbon N Y*, vol. 63, pp. 460–470, 2013, doi: <https://doi.org/10.1016/j.carbon.2013.07.017>.
- [57] J. A. Zimmerman, E. B. WebbIII, J. J. Hoyt, R. E. Jones, P. A. Klein, and D. J. Bammann, “Calculation of stress in atomistic simulation,” *Model Simul Mat Sci Eng*, vol. 12, no. 4, pp. S319–S332, Jun. 2004, doi: 10.1088/0965-0393/12/4/s03.

- [58] S. M. Hatam-Lee, A. Rajabpour, and S. Volz, “Thermal conductivity of graphene polymorphs and compounds: From C₃N to graphdiyne lattices,” *Carbon N Y*, vol. 161, pp. 816–826, 2020, doi: 10.1016/j.carbon.2020.02.007.